REPORT NO.
UCB/SEMM-94/17

STRUCTURAL ENGINEERING
MECHANICS AND MATERIALS

ANALYSIS OF FUNCTIONALLY GRADIENT POLYMER COMPOSITES

BY

A. H. Nashat
M. Ferrari
and
G. C. Johnson

JUNE 1994

DEPARTMENT OF CIVIL ENGINEERING
UNIVERSITY OF CALIFORNIA
BERKELEY, CALIFORNIA

ANALYSIS OF FUNCTIONALLY GRADIENT POLYMER COMPOSITES

Amir H. Nashat*, Mauro Ferrari*, and George C. Johnson**

*Department of Materials Science and Mineral Engineering
**Department of Mechanical Engineering
University of California, Berkeley

ABSTRACT:

Functionally graded copper- and tungsten-reinforced epoxy resin composites are fabricated via a casting technique. The driving force for grading is the density difference between the reinforcement and matrix phases. The reinforcement volume fraction profile is determined by measurement of local density. Reinforcement concentration is found to increase by 31 vol% for the copper plate and 22 vol% for the tungsten plate, with the majority of the increases occurring across transition regions into settling bands at the bottom of the plates. Stiffness profiles are also measured using ultrasonic wave propagation techniques, and compared with variational bounds on effective moduli. Comparison shows that homogenization methods predict plate stiffness accurately in the dilute regions, and under-predict stiffness, by 23% for the tungsten plate and 28% for the copper plate, in the high-concentration settling band regions. Our technique for density measurement is inaccurate in the transition regions due to the large gradients and small length scales. The measured volume fraction profiles for both plates are also used to demonstrate the ability of functionally grading to reduce thermal stresses in coated plates.

INTRODUCTION:

Composite materials have become a prominent material system in the engineering community because they enhance a variety of properties by combining two or more distinct, "homogeneous" material phases. Functionally gradient materials (FGM's) represent a novel twist to the field of composites by varying the distribution of the reinforcement phase with position in the material. Thus, effective macroscopic properties are not uniform, providing possible advantages in material behavior. The ultimate goal is to be able to tailor materials for specific applications. To achieve this end, we must determine both the effects of reinforcement gradients on material properties and the manufacturing processes that will produce such gradients.

To date, the greatest examples of FGM's can be found in nature: tree trunks; fruit peels; bones. The field of civil engineering boasts perhaps the most successful man-made FGM: reinforced concrete. Much effort is currently being placed to develop FGM's for numerous other engineering applications, particularly where large thermal, mechanical, and chemical gradients exist. Most promising of these applications appears to be the use of FGM's as advanced coatings and barriers, in the hope that the interface problems common to conventional coatings can be eliminated. New heat shield tiles on space-craft, for example, are functionally graded in the region between the glass coating and the insulation tile.[1] Silicon carbide/graphite FGM's have been developed to enhance the oxidation-resistance of graphite materials used in highly-oxidizing, high-temperature environments.[2] FGM's are also being investigated to improve ceramic joining and for use as pressure vessel walls.[3][4] Despite the large efforts into manufacture and application, however, the theoretical treatment of functionally gradient composites to determine effective field properties (e.g. elastic constants) is still under development.[5] Currently, only finite element solutions exist for analysis of the mechanical properties of FGM's. The problem exists, however, that point-wise application of effective medium theories (i.e. homogenization) used to analyze macroscopically homogeneous composites may be inaccurate in cases where gradients are large and a representative volume element (RVE) cannot be defined.[6]

In the following experiment, we treat both the manufacturing and theoretical modeling issues surrounding the development of FGM's. Functionally graded polymer composite plates reinforced with metal powders were fabricated by a casting technique. The concentration and elastic moduli gradients are experimentally determined via ultrasonic wave propagation. The elastic moduli are predicted through point-wise application of homogenization solutions, and comparison is then made between the predicted and measured stiffnesses. Finally, a theoretical study of the behavior of an FGM with the experimentally determined concentration profile exposed to thermal gradients is conducted. The goal of the study is two-fold: evaluation of the ability of this fabrication technique to produce functionally graded structures; and the applicability of homogenization theories.

MATERIALS:

Functionally graded plates were fabricated by a casting technique. Two types of metal powders were used as reinforcement: copper and tungsten. Micrographs have shown that the

copper powder is constituted of spheres varying from 5 to 40 microns in diameter. The tungsten appears to exhibit crystal planes as external surfaces, and varies in size between 0.5 and 5 microns. The polymer matrix is an epoxy resin (neat resin MY9512, provided courtesy of CIBA-GEIGY composites) mixed with a hardener (CIBA-GEIGY HT976, a 4-4 DDS) at a temperature varying between 93 °C and 99 °C. Once the resin was fully mixed, the metal powder was stirred in at a slightly higher temperature of 104 °C to facilitate full dispersion of the powder into the resin. The mixture was then placed in a vacuum at 121 °C to remove all gases and poured into vertical plate moldings (150 mm x 150 mm x 3 mm) preheated to 121°C. The castings were given a high-temperature curing treatment: 121°C until solidification (generally overnight); followed by 2.5 hours at 177 °C to complete the curing. A gentle cool-down cycle was necessary to prevent thermal shock cracking of the epoxy matrix.

Differences in the densities of the metal powder reinforcement and the polymer matrix allowed for settling of the reinforcement during the early stages of the curing phase. Various materials parameters affected the extent of settling. First, the two metal powders were chosen because of differences in their densities, 8.92 g/cm^3 for copper and 19.3 g/cm^3 for tungsten, compared to 1.26 g/cm^3 for the epoxy matrix, thus resulting in different driving forces for settling. In addition, the duration of the settling period and the viscosity of the resin were altered by addition of fixatropes and advancement of the resin before the reinforcement was added. In all, seven different plates were fabricated, each differing in one or more of the parameters specified above. Of these, the two plates that displayed the strongest concentration gradients, one copper-reinforced and the other tungsten-reinforced, were chosen for elastic property analysis.

To predict the local effective stiffness in the FGM's via the homogenization formalisms, the elastic moduli for the two fiber phases and the matrix phase are necessary. These were found in the literature to be: $E^{Cu} = 129.8$ GPa; $E^{W} = 407$ GPa; $\nu^{Cu} = 0.343$; $\nu^{W} = 0.2825$, where E is Young's Modulus and ν is Poisson's Ratio.[7] Poisson's Ratio for the epoxy matrix was found in the literature as 0.39;[8] Young's modulus was measured experimentally to be 5.3 GPa.

DEVELOPMENT OF PREDICTIVE MODELS:

The methods of homogenization are used to predict the elastic moduli of the FGM's at various points throughout the plates. The predicted stiffnesses will be accurate if the concentration gradients are small enough that the material surrounding each point can be considered homogeneous. If concentration gradients are too large, a representative volume element (RVE) of material which is both homogeneously reinforced and is sufficiently large with respect to the microstructural dimensions (i.e. particle size) cannot be defined. Hence, blind point-wise application of homogenization formalisms may lead to large inaccuracies. When comparing with experimental results, however, the complication arises that experimental techniques also average over a given region of material, introducing errors as well. Thus, the cause of a possible disparity between experimental and theoretical results, whether it be inapplicability of homogenization or experimental error, may not be obvious. The hope is to obtain large, smooth gradients that can be accurately measured and yet violate the requirements of homogenization.

The copper phase has a nearly perfect spherical shape; thus, it will be modeled as such. The tungsten phase is polyhedral; due to the limitations of the numerical software, this phase is also initially modeled as spherical. The further assumption is made that both metal phases and the resin matrix are isotropic.

Under the above assumptions, the two prominent homogenization schemes, the Mori-Tanaka and the poly-inclusion formalisms, become equivalent.[9][10] In addition, if the matrix phase is the softer phase, as is the case with our FGM's, then both predictive models coincide with the Hashin-Shtrikman lower bound. For simplicity, we use the variational bounds for comparison with experimental results. The explicit expressions for these bounds are:

$$\frac{(K_f - K_m)\alpha}{1+\left[(1-\alpha)\frac{K_f - K_m}{K_m + K_L}\right]} + K_m \le K \le \frac{(K_f - K_m)\alpha}{1+\left[(1-\alpha)\frac{K_f - K_m}{K_m + K_U}\right]} + K_m$$
$$\frac{(G_f - G_m)\alpha}{1+\left[(1-\alpha)\frac{G_f - G_m}{G_m + G_L}\right]} + G_m \le G \le \frac{(G_f - G_m)\alpha}{1+\left[(1-\alpha)\frac{G_f - G_m}{G_m + G_U}\right]} + G_m \qquad (1)$$

where K and G indicate bulk and shear modulus, respectively, and α is the fiber volume fraction.[11] The subscripts "m" and "f" designate the matrix and fiber phases. For our FGM samples, the condition exists that $(G_f - G_m)(K_f - K_m) \ge 0$, resulting in the following relations:

$$K_L = \frac{4}{3}G_m$$
$$K_U = \frac{4}{3}G_f$$
$$G_L = \frac{3}{2}\left(\frac{1}{G_m} + \frac{10}{9K_m + 8G_m}\right)^{-1} \qquad (2)$$
$$G_U = \frac{3}{2}\left(\frac{1}{G_f} + \frac{10}{9K_f + 8G_f}\right)^{-1}$$

As seen in Equation 1, once the local reinforcement volume fraction is known, the local stiffness can be predicted. Density measurements determine the reinforcement volume fraction, detailed in the Experimental Procedure section below. For non-spherical particle shapes and anisotropic material properties, the Hashin-Shtrikman bounds no longer coincide with homogenization predictions, and one of the formalisms, either Mori-Tanaka or poly-inclusion, should be explicitly utilized.

EXPERIMENTAL PROCEDURE:

The two experimentally determined values are the local reinforcement volume fraction (α) and the local stiffness. Both values are found at various points in the plate along the direction of the grading. The local volume fraction is determined through measurement of the local material density (ρ_{eff}). Small tetrahedra (25 mm x 5 mm x 3 mm) are cut out of a strip (130 mm x 25 mm) in the center of the plate, as shown in Figure 1. Weight and volume measurements of the tetrahedra provide ρ_{eff}, which is related to α via the relation:

$$\alpha = \frac{\rho_{eff} - \rho_m}{\rho_f - \rho_m} \tag{3}$$

The local stiffness modulus is determined via local ultrasonic wave velocity measurements using a double-pulse echo system.[12] Ultrasonic waves with frequencies between 4 an 7 MHz are propagated through the thickness of the plates over the 130 mm x 25 mm region indicated in Figure 1. The origin indicated in Figure 1 is utilized for positioning the ultrasonic scan. All y co-ordinate positions specified in the remainder of this paper will be with respect to this origin and co-ordinate system. Measurements are performed in water so that the plate can be scanned automatically. Shifts in the frequency of the wave (f) as it propagates through the plate, with a constant phase shift between transmitted and reflected waves, are measured. For small frequency changes, the shift in frequency can be related to changes in velocity (V) via:

$$\frac{\Delta V}{V_o} = \frac{\Delta f}{f_o} + \frac{\Delta d}{d_o} \tag{4}$$

where d is the distance the wave has propagated (i.e. twice the plate thickness). The velocity at the starting point of the scan (V_o) is measured, and hence the velocity at all points in the scanned region of the plate can be determined. The relation between wave velocity and stiffness is given by:

$$\left[\left(C_{ijkl} + T_{il}\delta_{jk}\right)n_i n_l - \rho_{eff}V^2\delta_{jk}\right]U_k = 0 \tag{5}$$

where **U** is the wave amplitude vector, **n** is the unit vector in the direction of propagation, and δ_{ij} is the Kronecker Delta.[12] Because the plates are thin, one can assume the stress is zero (T_{ij}), and with the further assumption of a pure longitudinal mode wave propagating through the plate, the stiffness-velocity relation simplifies to:

$$C_{11} = \rho_{eff}V^2 \tag{6}$$

where we have taken the "1" direction as perpendicular to the plate face, and we have recast the stiffness tensor (C_{ijkl}) as a 6x6 matrix, C_{ij}. Thus the experimentally determined elastic modulus is C_{11}. This value can be compared directly with the bounds of Equation 1 given the extra relation:

$$C_{11} = K + \frac{4}{3}G \tag{7}$$

The calculation of stiffness requires the measurement of frequency shift, plate thickness (equivalent to d/2 in Equation 4) and local density. Throughout the majority of the plate, frequency shift is measured at 1 mm intervals along the plate in the grading direction. The density is measured at 5 mm intervals, and the plate thickness every 10 mm. These latter two values are interpolated between data points to allow calculation of stiffness every 1 mm. Near the bottom of the plate frequency shift cannot be measured 1 mm intervals because of edge effects and sudden changes in concentration where settling bands have formed. Hence, in this region of the plate, experimentally determined stiffness profiles are more coarse. Again, linear interpolation of the density and thickness measurements are performed where necessary.

The local density measurements are also used in the prediction of the local stiffnesses, as α is needed in Equation 1. Since the local density is measured at 5 mm intervals, the predictions of C_{11} will also be every 5 mm. Note that the accuracy of these predictions is based on both the accuracy of the theoretical models and the uncertainty in the measurements of local density.

The uncertainty in the calculation of local stiffness is a function of uncertainties in the wave velocity and local density measurements. The uncertainty in wave velocity is due to the uncertainties in the start point velocity (V_o) and $\Delta V/V_o$. These uncertainties are small: $\pm 0.3\%$ and $\pm 0.2\%$, respectively. The uncertainty in the calculation of wave velocity is thus $\pm 0.4\%$. The accuracy of the calculation of local density is a function of the uncertainties in measurements of the mass and volume of the tetrahedra removed from the plates. The measurement of mass is extremely accurate, with a maximum uncertainty of $\pm 0.07\%$. The uncertainty in measurement of volume is dependent on position in the samples. In the central region of the plates, the tetrahedra were machined so that uncertainty in measurement of all three length dimensions is less than $\pm 1\%$. The total uncertainty in volume measurements in the central portion of the plates is $\pm 1.1\%$. resulting in an uncertainty in local density of $\pm 1.1\%$ as well. However, at the bottom of the plates, the tetrahedra were necessarily smaller, so as to fall within settling bands. The uncertainty in volume and local density measurements in this region of the samples is $\pm 3\%$. Thus, uncertainty in density measurement is $\pm 1.1\%$ throughout the central portion of the plates, and increases to $\pm 3\%$ at the bottom. The resulting uncertainty in the local stiffness calculation is $\pm 1.5\%$ throughout the majority of the FGM samples, increasing to $\pm 3.5\%$ at the base.

RESULTS AND DISCUSSION:

Two FGM plates (one carbon-reinforced, the other tungsten-reinforced) exhibiting the largest frequency shifts ($\Delta f/f_o$) from the top of the plate to just above the settling bands were chosen for experimental analysis. The frequency shift for the copper FGM was -4%, for the tungsten -5.5%. All other FGM samples exhibited frequency shifts smaller in magnitude than 2.5%. Note that $\Delta f/f_o$, and correspondingly $\Delta V/V_o$, are increasingly negative with increases in volume fraction, indicating that velocity decreases with increasing reinforcement. This result is expected in the low concentration regime, as the increase in density with an increase in volume fraction outweighs the resulting increase in stiffness, thus necessitating a reduction in velocity (see Equation 6). Based on the expression for the Hashin-Shtrikman lower bound, velocity is expected

to decrease up to a fiber concentration of 38 vol% for copper-reinforced epoxy, and up to 42 vol% for tungsten-reinforced epoxy.

The combination of the frequency shift and the measured changes in plate thickness ($\Delta d/d_o$) allowed for calculation of wave velocity profiles, shown in Figure 2. As expected, the velocities decreased with increasing α, from 2900 m/s to 1900 m/s for the tungsten FGM, and from 2850 m/s to 2350 m/s for the copper plate. The sudden drops in velocity at the bottom of both FGM's is due to the presence of settling bands. As can be seen in Figure 2, the tungsten-reinforced FGM exhibited an extremely well-defined transition from the epoxy-rich region into the settling band. The copper FGM shows a less well-defined transition. Note the minimum in the velocity through the copper plate at y = -132 mm. This phenomenon is attributed to either a local increase in α, or to the minimum in velocity predicted by the Hashin-Shtrikman lower bound. As will be seen below, the fiber concentration at this position is close to the fiber fraction at which the lower bound predicts the minimum will occur; and no local increase in ρ_{eff} was observed.

The measurements of local density provided volume fraction profiles, shown graphically in Figure 3. As seen in Figure 3a, the copper-reinforced FGM has higher fiber fractions at all positions than the tungsten FGM, with a maximum of 32 vol% at the bottom of the plate. The tungsten-reinforced plate shows a sharper transition into the settling band, but has a maximum of only 22 vol% at the base. Figure 3b shows the profiles over the epoxy-rich region of the plates, prior to transition into the settling bands. The volume fraction profiles appear linear and smooth. The gradients, however, are extremely small: 2.5 vol%/100 mm for the copper FGM; and 1 vol%/100 mm for the tungsten FGM. Unfortunately, at positions in the plates where changes in concentration are large, the length scales are extremely small. In both FGM samples, α increases by one order of magnitude across the transition region, a distance of 1 mm for the tungsten plate and 5 mm for the copper plate. The result is large errors in local density measurement and interpolation. A happy medium could not be found where large, smooth, experimentally measurable volume fraction gradients existed. During manufacturing, we increased resin viscosity to eliminate settling bands; the result was a series of relatively homogeneous composite plates with almost no gradients.

The local density measurements were combined with the wave velocity profiles to calculate local stiffness. The C_{11} profiles are given in Figures 4 and 5 for the copper and tungsten FGM's, respectively. Figures 4a and 5a show the epoxy-rich region. The Hashin-Shtrikman lower bound, and consequently homogenization predictions, show good agreement with the experimental values within experimental uncertainty. Unfortunately, increases in stiffness are small, from 10.5 to 11.1 GPa for the copper FGM, and from 10.7 to 10.95 GPa for the tungsten FGM.

The stiffness profiles in the transition and settling band regions are given in Figures 4b and 5b. The experimentally determined stiffness falls within the bounds at all points, but diverges from the lower bound as the transition is made into the settling bands; the Hashin-Shtrikman lower bound under-predicts C_{11}, by 28% for the copper FGM and 23% for the tungsten FGM. This divergence falls outside the experimental uncertainty, and volume fractions are still within the dilute regime where homogenization is valid. Thus, we believe that the steep gradients of the

transition region play some role in the observed disparities. The sudden peak exhibited in Figure 5b at y = -137 mm is most probably due to the large errors introduced by interpolating between density measurements at the transition region. All stiffness predictions between y = -130 mm and y = -138 mm seem to exhibit this error. As noted above, in regions where stiffness changes are appreciable, length scales are too small for our density measurement technique. Thus, the theoretical models (bounds and homogenization) predict stiffness extremely well in the dilute central portions of the plates, under-predict stiffness in the settling bands, and no results can be drawn in the transition regions.

To confirm the benefits of graded coatings over traditional discontinuous coatings, the behavior of FGM plates with the volume fraction profiles of Figure 3 subject to thermal gradients were studied theoretically. For this study, the plates are graded in the z direction, with the high reinforcement concentration at z = 0 mm and the low reinforcement at z = 130 mm; the plates are infinite and homogeneous in the x and y directions. A temperature of 100 °C is imposed on the surface at z = 0 mm, and a temperature of 0 °C is maintained at z = 130 mm. Figure 6 shows the results obtained for the tungsten-coated epoxy plates. Two types of discontinuous coatings were employed: one of pure tungsten with a thickness of 2.1 mm; and the other of 21 vol% tungsten with a thickness of 10 mm. Note that all three plates have the same total volume fraction of tungsten. As can be seen in Figure 6a, temperature gradients are nearly identical in all three structures. The advantage to grading is realized in the in-plane stress distribution profiles, shown in Figure 6b. The stresses in the FGM plate are approximately two orders of magnitude lower than in the 2.1 mm coated structure, and up to a factor of three lower than in the 10 mm coated plate. Note that the FGM is not pure tungsten on the top surface, a condition which may be required depending on the application; however, the advantage to grading is clear. Figure 7 shows similar results for copper coated plates; the discontinuous coating is pure copper, 4.1 mm thick. Again, temperature gradients are indistinguishable in both cases (Figure 7a), while stresses in the graded coating are lower by almost two orders of magnitude than those in a pure coating (Figure 7b).

CONCLUSIONS:

We fabricated and studied metal powder-reinforced epoxy FGM's in an attempt to determine the viability of our casting technique for creating FGM's and the applicability of homogenization techniques to these material systems. As shown in Figure 3, the composite plates are definitely graded in the y-direction. However, the grading is not smooth and continuous along the entire plate. Instead, there exists a large epoxy-rich region occupying the majority of the plate where concentration and stiffness gradients are extremely small. This dilute region is separated from the high-concentration, high-stiffness settling bands at the bottom of the plates by a narrow transition region. Volume fractions increase by one order of magnitude across the transition region, over a distance no greater than 5 mm. Attempts to eliminate settling bands during the fabrication process were unsuccessful. The volume fraction profile of Figure 3 is in effect the desired result for coating applications, where the grading at the transition region helps reduce interface problems. However, for our purposes of comparison with homogenization, the steep gradients introduced large errors in measurement of local density in these regions.

The experimentally determined stiffness, C_{11}, was compared with predictions of the Hashin-Shtrikman variational bounds. The experimental results fell within the bounds at all points along the plates. In the dilute region, agreement between experimental results and the lower bound (coincident with homogenization predictions) was within the experimental uncertainty. In the high concentration settling region, however, the lower bound under-predicted the stiffness. No results could be drawn for the transition regions because of the large errors associated with local density measurement. The α profiles of Figure 3 were also used to illustrate the advantage of functional grading in reducing thermal stresses. As shown in Figures 6 and 7, thermal stresses were reduced by two orders of magnitude when a pure, discontinuous coating was replaced by the graded structure, and by up to a factor of three when a 21 vol% discontinuous coating was replaced by the graded structure possessing the same surface volume fraction.

REFERENCES:

1. D.B. Leiser, R. Churchward, V. Katvala, and D. Stewart. "Advanced porous coating for low-density ceramic insulation materials," *Journal of the American Ceramic Society*, vol. 72, no. 6, pp. 1003-1010 (1989).

2. K. Fujii, H. Imai, S. Nomura, and M. Shindo. "Functionally gradient material of silicon carbide and carbon as advanced oxidation-resistant graphite," *J. of Nuclear Materials*, 187, 3, pp. 204-208 (1992).

3. B.J. Dalgleish, M.R. Locatelli, A.P. Tomsia, et al. "Transient liquid phase bonding approaches for ceramic joining." Submitted to First International Conference on Composites Engineering (1994).

4. P. Kwon. "Macroscopic fabrication and design of functionally gradient materials," PhD. Dissertation, Department of Mechanical Engineering, University of California, Berkeley (1994).

5. J. Zuiker and G. Dvorak. "The effective properties of functionally graded composites -- I. Extension of the Mori-Tanaka method to linearly varying fields," *Composites Engineering*, 4, 1, pp. 19-35 (1994).

6. J. Aboudi, S.M. Arnold, and M. Pindera. "Response of functionally graded composites to thermal gradients," *Comp. Eng.*, 4, 1, pp. 1-18 (1994).

7. *Metals Handbook, 10th Edition, Vol.2: Properties and Selection: Non-ferrous Alloys and Special Purpose Materials*. ASM International, Metals Park, Ohio, 1990.

8. D. Hull. *An introduction to composite materials*. Cambridge University Press, Cambridge, 1981, pp.28-32.

9. G.J. Weng. "Some elastic properties of reinforced solids with special reference to isotropic ones containing spherical inclusions," *International Journal of Engineering Science*, 22, pp. 845-856 (1984).

10. M. Ferrari. "Composite homogenization via the equivalent poly-inclusion approach." *Comp. Eng.*, 4, 1, pp. 37-45 (1994).

11. R.M. Christensen. *Mechanics of Composite Materials*. Kriegar Publishing Company, Florida, 1991, pp. 106-118.

12. G.C. Johnson and W.C. Springer. "A comparison of measured and predicted second- and third-order elastic constants of a textured aggregate," *International Journal of Solids and Structures*, 25, 6, pp. 609-619 (1989).

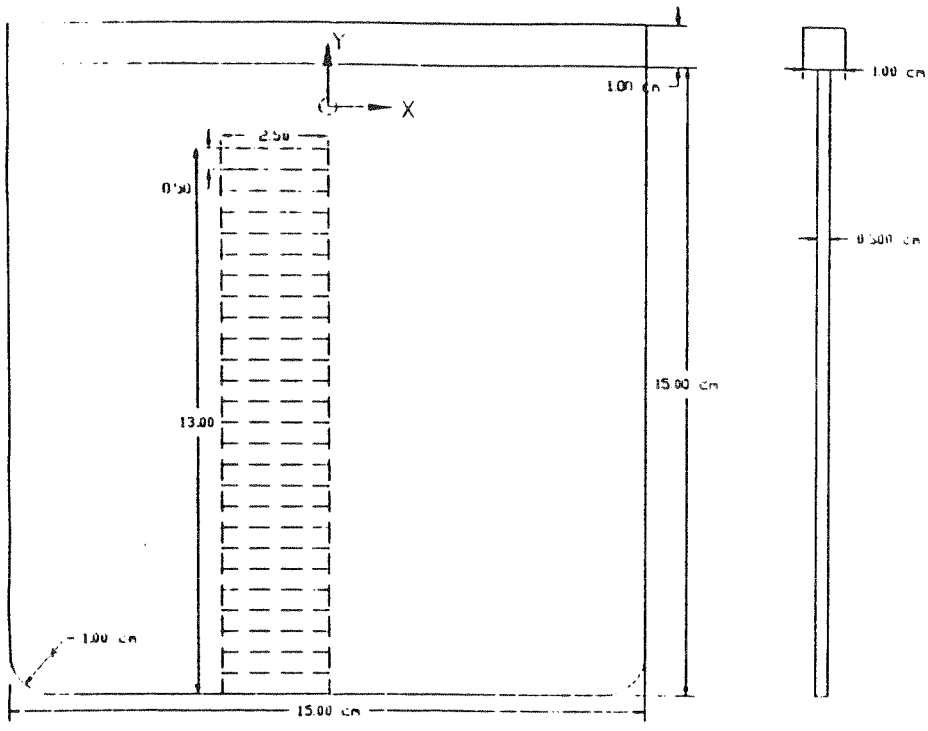

Figure 1: Schematic of FGM plate; dashed lines mark regions in specimen that were removed for experimental analysis. All dimensions are in centimeters.

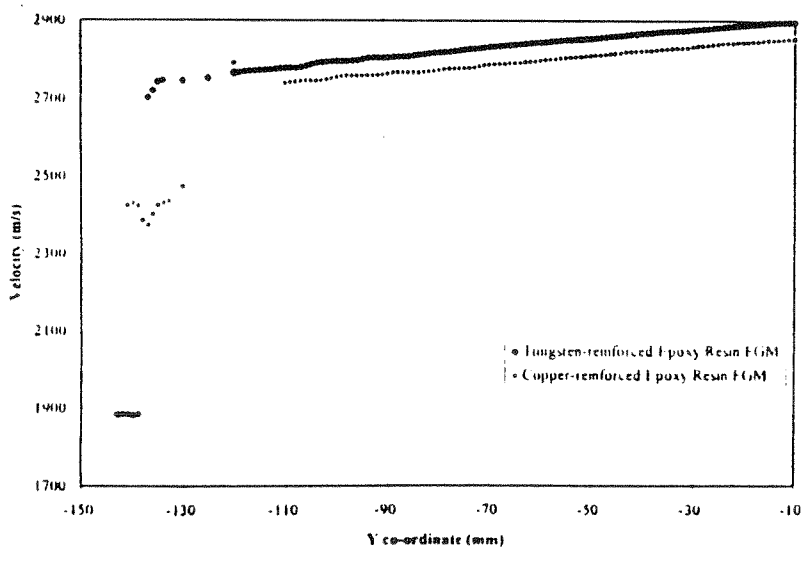

Figure 2: Wave velocity profiles for tungsten- and copper-reinforced FGM plates.

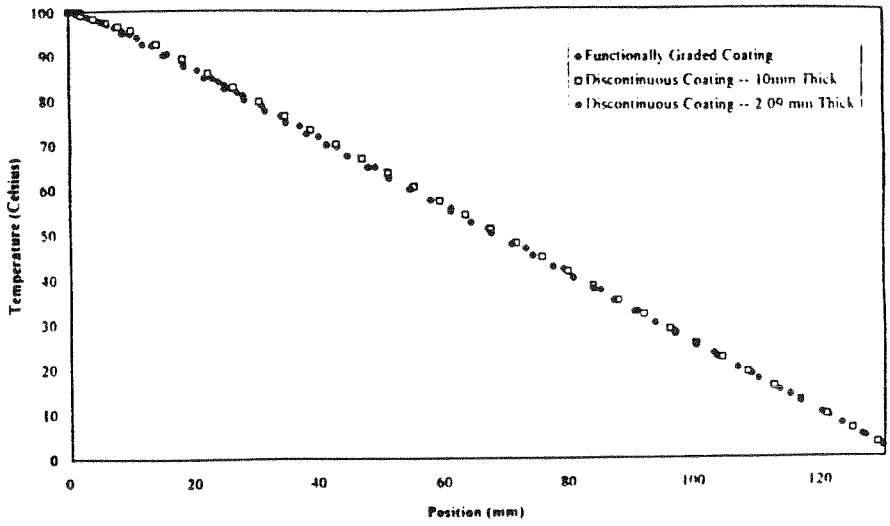

Figure 6a: Temperature profile for tungsten-coated epoxy plates.

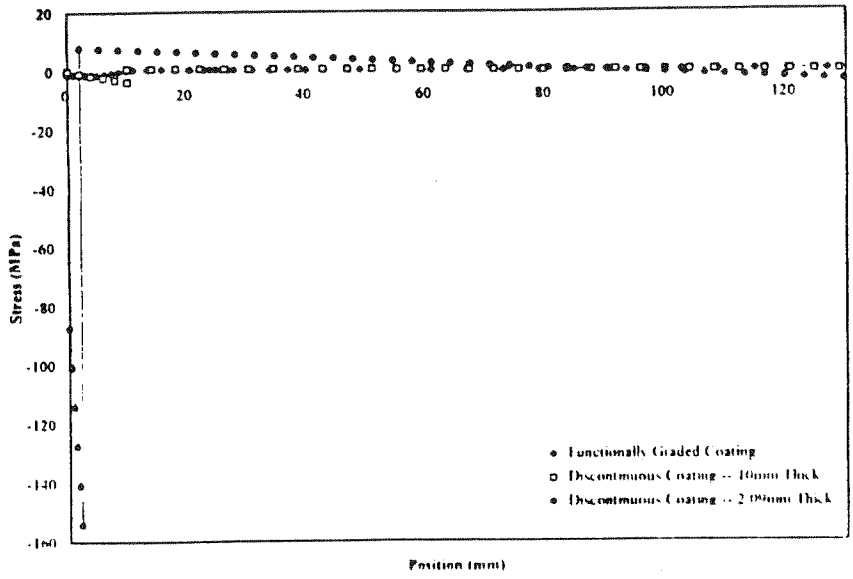

Figure 6b: Thermal stress profile for tungsten-coated epoxy plates.

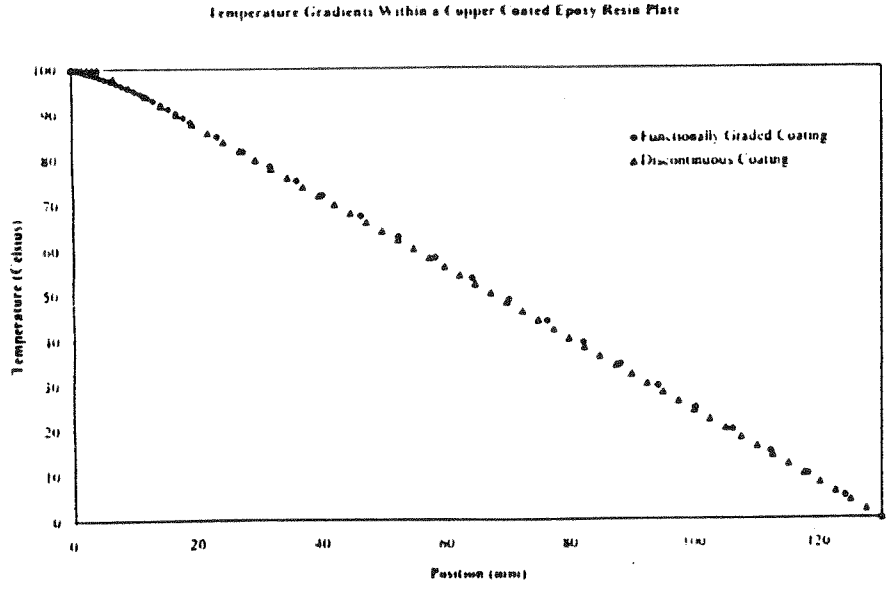

Figure 7a: Temperature profile for copper-coated epoxy plates.

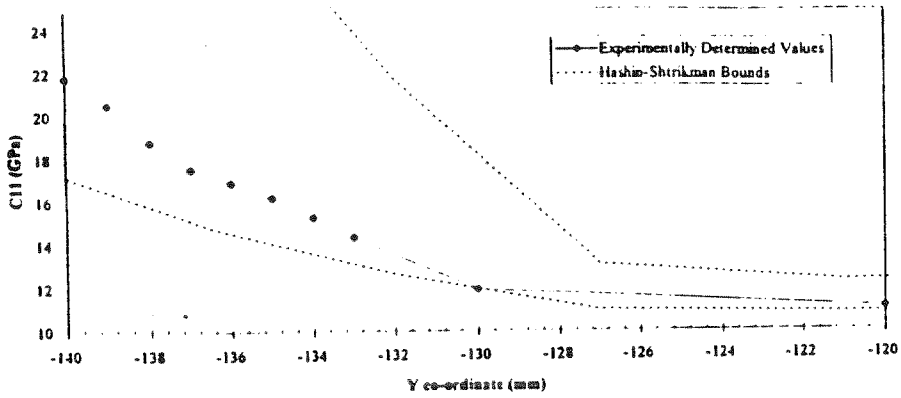

Figure 4b: Stiffness (C_{11}) profile for the copper-reinforced FGM plate over the transition and settling band regions.

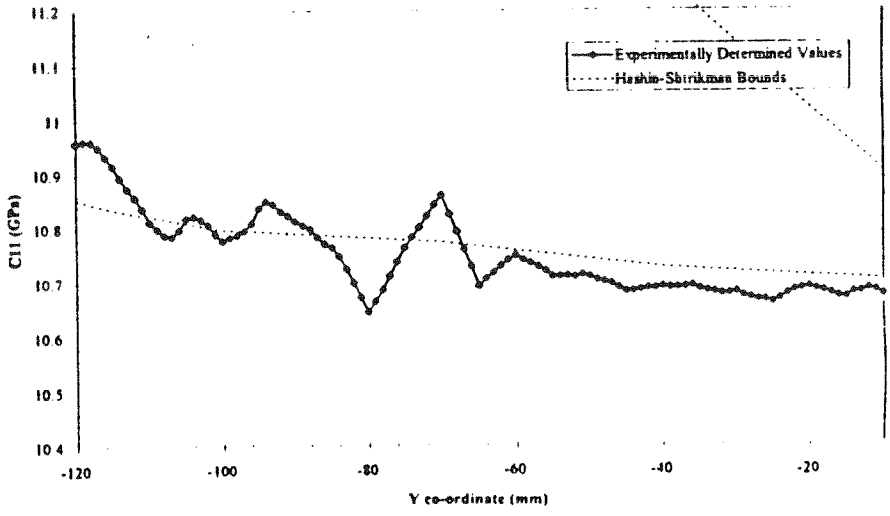

Figure 5a: Stiffness (C_{11}) profile for the tungsten-reinforced FGM plate over the dilute region.

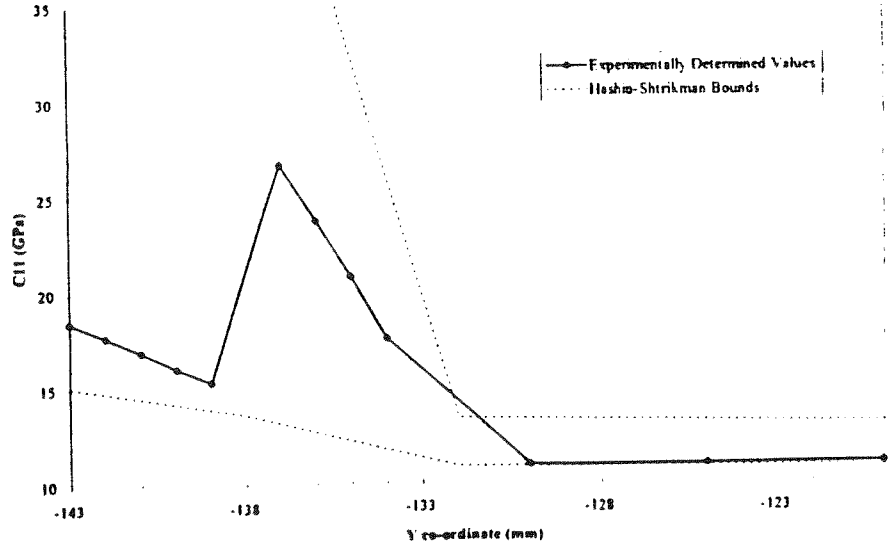

Figure 5b: Stiffness (C_{11}) profile for the tungsten-reinforced FGM plate over the transition and settling band regions.

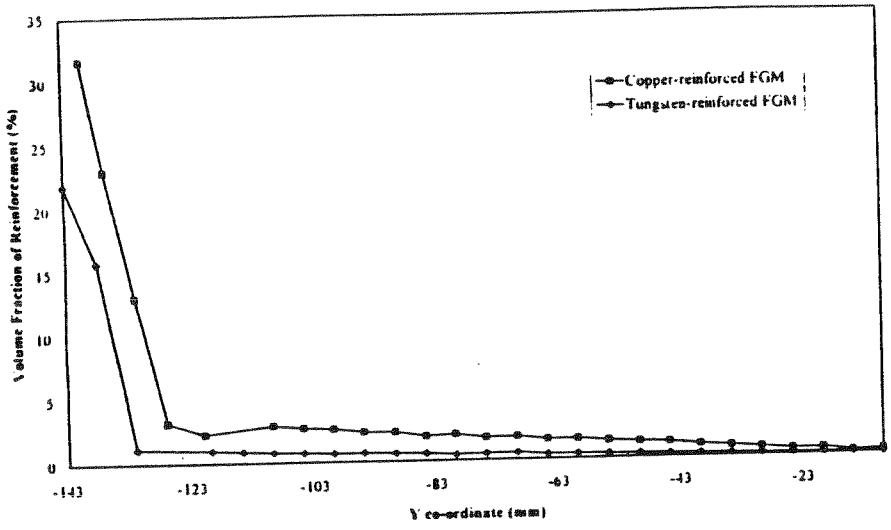

Figure 3a: Volume fraction profiles for tungsten- and copper-reinforced FGM plates over the entire region of study.

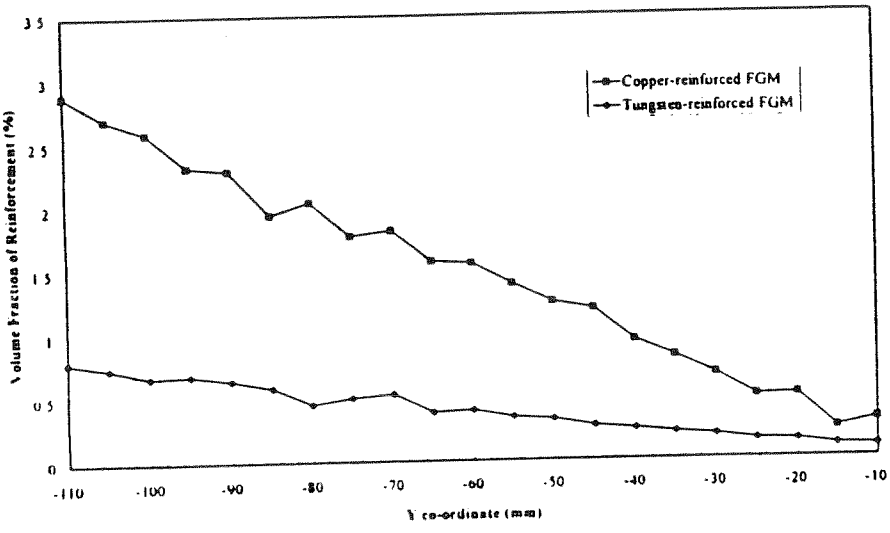

Figure 3b: Volume fraction profiles for tungsten- and copper-reinforced FGM plates over the dilute region.

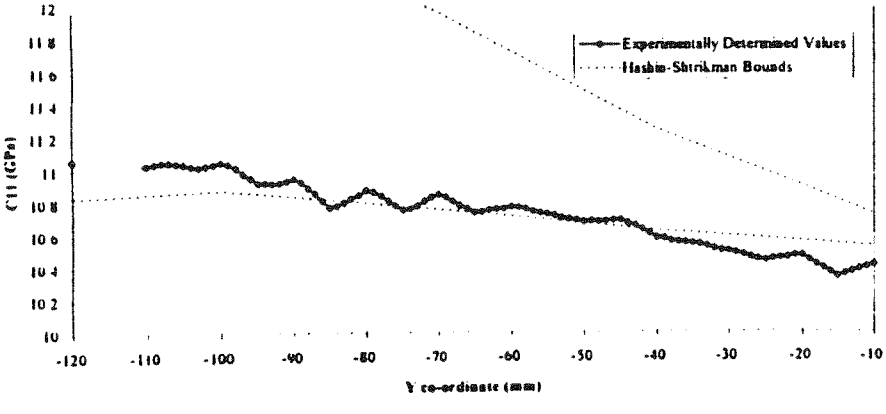

Figure 4a: Stiffness (C_{11}) profile for the copper-reinforced FGM plate over the dilute region.

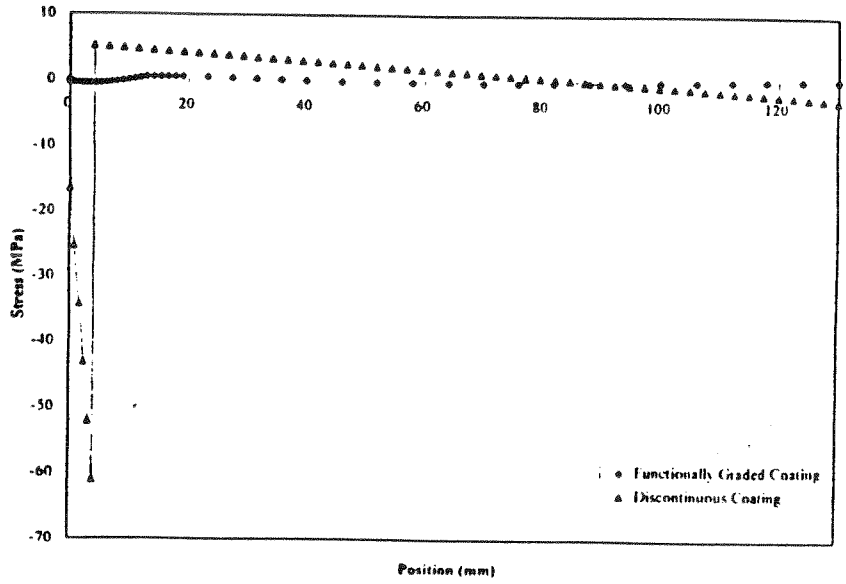

Figure 7b: Thermal stress profile for copper-coated epoxy plates.